Heliyon 10 (2024) e34267

Contents lists available at ScienceDirect

Heliyon

journal homepage: www.cell.com/heliyon

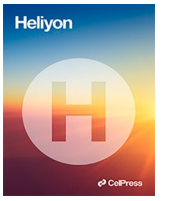

Research article

MnO_2 decoration onto the guava leaves: A sustainable and cost-effective material for methylene blue dye removal

Noufal Komby Abdulla [a,1], Elham A. Alzahrani [b,1], Poonam Dwivedi [c], Shruti Goel [c], Sumbul Hafeez [d], Mihir Khulbe [c], Sharf Ilahi Siddiqui [c,*], Seungdae Oh [e,**]

[a] Department of Chemistry, Jamia Millia Islamia, New Delhi-110025, India
[b] Department of Chemistry, College of Science, University of Ha'il, Ha'il 81451, Saudi Arabia
[c] Department of Chemistry, Ramjas College, University of Delhi, Delhi-110007, India
[d] Department of Civil and Environmental Engineering, Villanova University, 800 E, Lancaster Ave, Villanova, PA, 19085, USA
[e] Department of Civil Engineering, Kyung Hee University, Yongin-si 17104, Gyeonggi-do, South Korea

ARTICLE INFO

Keywords:
Water
Pollutant
Water treatment
Adsorption
Nanocomposite
MnO_2
Guava leaves

ABSTRACT

Excessive number of dyes in water is becoming the main cause of water pollution, which is very important to remove because it is harmful. Dye contaminated water is being treated by various methods. Adsorption method can be considered best for the study of dye removal due to several technological reasons. The adsorption method has also been emphasized in this study. In the present work, a nano-bio-composite was fabricated by growing manganese oxide nanoparticles on abundant cellulosic guava leaf powder. This allows nanocomposite to be prepared in large quantities at nominal cost. The characterization technique confirmed the irregular growth of manganese oxide nanoparticles onto the guava leaf powder. The electrostatic and non-electrostatic interactions was confirmed in between manganese oxide nanoparticles and the carbon structure of guava leaf powder. The massive functional groups were found to be in the prepared nano-bio-composite. The grain size of prepared material was in nano range. The developed nano-bio-composite was used to remove methylene blue from water. This showed a very good adsorptive capacity for methylene blue. The analyzed adsorption data was modelled through isotherms, kinetics and thermodynamics models. The nature of the adsorption process was determined to be spontaneous and exothermic. The reusability test was carried out for five adsorption-desorption cycles. The reusability results suggested the better removal efficiency (%) in the first two cycles with only 20 % reduction in removal efficiency (%). The leaching test result revealed the good stability of MnO_2/GL at neutral pH. It was a unique and cheap adsorbent of its kind, which had not been noticed anywhere before.

1. Introduction

Water is one of nature's most precious gifts essential for life, however extensive industrialization has raised serious environmental concerns [1]. Disposal of untreated industrial waste and effluents into water bodies is posing a threat to living organisms and nature

* Corresponding author.
** Corresponding author.
E-mail addresses: sharf_9793@rediff.com (S. Ilahi Siddiqui), soh@khu.ac.kr (S. Oh).
[1] Both the authors contributed equally.

https://doi.org/10.1016/j.heliyon.2024.e34267
Received 27 March 2024; Received in revised form 27 June 2024; Accepted 6 July 2024
Available online 9 July 2024

[2]. Among various effluents, dyes are found to be significant contaminants in wastewater [3,4]. Approximately 10 % of the 70 million tons synthetic dye produced is annually discharge into the aquatic environment in the form of wastewater [5]. These dyes pose a threat to the life of living organisms and sustainability of nature due to their non-biodegradability, presence of heavy metals in their structure, and their decomposition into carcinogenic metabolites [6]. Among the various dyes, methylene blue (MB) is highly persistent, bio-accumulative and toxic [7,8]. Exposure to MB can cause adverse health effects in humans, including skin irritation, respiratory problems, and possibly eye damage [8]. Ingestion or inhalation of high concentrations of MB can be particularly dangerous and may lead to more serious health complications [9]. Therefore, wastewater treatment is a crucial process for removing toxic elements such as MB from wastewater, enabling wastewater reuse, and preventing waste accumulation.

Various wastewater treatment technologies (biological, physical and chemical) are being developed to remove pollutants from wastewater [4,10,11]. Among these, adsorption method has been found to be a promising method for the pollutant removal from wastewater [10]. In this process, adsorbate (pollutant) molecules adsorb onto the surface of the adsorbent via chemo or physio interaction [12]. In terms of the ease of operation, fastness, insensitivity to toxic pollutants, flexibility, and the initial cost of adsorbents, adsorption is found to be superior to other methods [10,12]. However, the efficiency of this process is highly influenced by the size, shape, surface area, and nature of the adsorbent [10,12]. There is an extensive range of adsorbents that can be employed for the water remediation [10,12,13]. These include activated carbon [14], metal-organic frameworks (MOFs) [15–17], metal or metal oxide-based nanomaterials (NMs) and others [18–20].

Nano-adsorption method using nanoparticles (NPs) has emerged as a powerful wastewater treatment technology [18]. Owing to the increased surface-to-volume ratio, high porosity, and improved properties compared with bulk, NPs have high adsorption properties for the removal of dyes from wastewater [18–20]. Considering the utility and demand of NPs in wastewater treatment, many efforts are being made to increase the production of these NPs at low cost. Modern research shows that by combining NPs with other materials, their cost can be reduced and their production and adsorption efficiency can be increased [21]. Activated carbon (AC)-based NMs are proving to be quite useful for conventional dye removal processes. AC has attractive adsorption capacities due to its high thermal and chemical inertness, well-defined adsorption sites, and large surface area-to-volume ratio [22]. By merging AC with NPs, the resulting AC-based NMs have the many additional properties such as high porosity, large surface area, large functional groups, magnetic properties, optical properties etc., which makes the overall adsorption process more efficient [22,23]. However, the production of ACs requires a lot of heat and energy (high temperature electric furnace) and toxic chemicals which increases the cost of ACs and is also responsible for additional air pollution [24]. Moreover, the low regeneration ability of AC-based NMs makes them less suitable for wastewater treatment purpose. To meet the idea of sustainability, researchers thereby are shifting their focus from AC-based NMs to biomass-based NMs [25]. Biomass is globally available in bulk and at affordable prices without any additional treatment. Biomass such as plant seeds, leaves, etc. contain many functional groups due to their cellulosic surface and also contain phytochemicals that facilitate the growth of NPs on their surface, and form a stable composite by forming strong bond with the NPs [25].

The global need to find novel methods which can function as an aid in wastewater treatment on the lines of sustainability makes this study a topic of concern. This study involves a new type of composite material based on natural biomass such as Psidium guava. Guava is a tropical plant that can be easily found around the world [26]. The high bioavailability of this plant makes it a suitable choice for its use in production of biomass based NMs [25]. In addition, the availability of essential phytochemicals including alkaloids, tannins, essential oils, etc. in the plant enhances its efficacy [26].

The novelty of this research lies from the novel application of Psidium guajava (guava) leaves decorated with MnO_2 NPs for wastewater treatment. This approach utilized the high bioavailability and rich of essential phytochemicals in guava leaves, to improve their effectiveness in contaminants removal [27]. Furthermore, the employing MnO_2 as a transition metal oxide offers several benefits such as cost-effectiveness, wide spread availability, and environmental compatibility [28]. The resultant nanocomposite (NC) exhibits diverse capabilities, combining the natural carbon source's multiple functional groups with MnO_2 strong oxidizing and photocatalytic properties [28]. This innovative approach provides a novel solution for water treatment, highlighting the integration of natural materials and cutting-edge nanotechnology.

2. Material and methods

All the materials used in this research are given in the supporting file (ESI).

2.1. Preparation of MnO_2/GL NC

After being washed and dried for 24 h at 90 °C in an oven, guava leaves (GL) were ground into a powder, sieved to separate granules, and kept in a desiccator for additional processing. Composite preparation was done by taking 1.0 g of GL in 100 mL of a 0.1 M $MnCl_2$ solution, followed by dropwise addition of 100 mL of 0.1 M $KMnO_4$ solution. The mixture was stirred for 45 min, at 60 °C, 650 rpm, and then was allowed to cool down to room temperature. The resulting MnO_2 precipitate was formed on the surface of GL, so the MnO_2/GL composite formation occurred [29]. The sample was collected by Whatman filtration, and was subjected to multiple washing cycles with deionized water for thorough cleaning. The compound was dried in a hot air oven at 65 °C for 60 h, and was then put to use for further characterization and adsorption studies.

2.2. Instrumentation and characterization

The prepared magnetic sample's physiochemical properties were examined with the help of a range of characterization methods and instruments, as mentioned in the Supplementary information file, ESI.

2.3. Batch adsorption experiments

The preparation procedure of MB stock solution for the present adsorption study is given in the ESI. To investigate MB adsorption behavior onto solid surfaces, batch adsorption tests were conducted. In this experiment, a known concentration of MB solution (10 mg L^{-1}) is mixed with a solid adsorbent material (MnO_2/GL, 1.0 g/L) and allowed to equilibrate. The concentration of the dye in the solution both before and after adsorption is then used to calculate the amount of dye adsorbed onto the solid surface.

The formula used for these analyses are [30]:

$$Adsorption\ capacity = (C_o - C)V / m \tag{1}$$

$$Adsorption\ \% = \{(C_o - C) / C_o\}\ x\ 100 \tag{2}$$

Where, C_o and C are before and after adsorption concentration in dye solutions, m is the mass of adsorbent material taken in gram, and V is the volume in liter.

The adsorption performance of MnO_2/GL was optimized at various conditions as discussed in the result and discussion section.

2.4. Adsorption thermodynamics and isotherms models

Thermodynamic theory is used to explain the adsorption process and understand its underlying principles. It involves the application of thermodynamic concepts, such as Gibbs free energy (ΔG), enthalpy (ΔH), and entropy (ΔS), to describe the energetics and spontaneity of the adsorption process.

The above-mentioned thermodynamic parameters can be calculated using the Van't Hoff equation and can provide insights into the spontaneity and energetics of the adsorption process. The Van't Hoff equation is given as [29]:

$$\Delta G = \Delta H - T\Delta S \tag{3}$$

$$\Delta G = -RT\ ln(K) \tag{4}$$

Where R is the gas constant, T is the temperature in Kelvin, and K is the equilibrium constant obtained from the adsorption isotherm.

Thermodynamic analysis can help in understanding the driving forces and mechanisms of dye adsorption, as well as in predicting the feasibility and efficiency of adsorption processes under different conditions.

The adsorption process was analyzed using adsorption isotherms, which explain the correlation between the equilibrium dye concentration in the solution (C) and the quantity of dye adsorbed (q). The Freundlich and Langmuir adsorption isotherms are employed for these studies.

The Langmuir isotherm assumes a monolayer adsorption and suggests that the adsorption occurs through specific sites on the adsorbent surface. The Langmuir isotherm equation is given as [30]:

$$q = (q_m \times b \times Ce)\ /\ (1 + b \times C) \tag{5}$$

Where, q_m is the maximum adsorption capacity of adsorbent, and b is the Langmuir constant associated with the adsorption energy.

The Freundlich isotherm, on the contrary, postulates multilayer adsorption and implies that adsorption takes place across a heterogeneous surface with distinct adsorption energies. The equation for Freundlich isotherm is provided as [30]:

$$q = K_F \times C^{1/n} \tag{6}$$

Where K_F is the Freundlich constant associated with the adsorption capacity, and n is the Freundlich exponent describing the heterogeneity of the surface.

2.5. Adsorption kinetic models

The two models utilized to examine the adsorption kinetics of MB onto the MnO_2/GL surface are pseudo first order kinetics and pseudo second order kinetics.

The underlying assumption of pseudo first order kinetics model is the rate of adsorption is directly correlated with the gradient between the initial concentration and time.

The equation for pseudo-first order kinetics is as follows [30]:

$$\log(C_o / C_t) = log\ C_o\ -\ (k_1 / 2.303)t \tag{7}$$

where the pseudo first order kinetics rate constant is denoted by k_1. A linear relationship can be seen by plotting log (C_o / C_t) against time (t), with the slope of the line representing the rate constant, k_1.

The pseudo second-order kinetics model postulates that the rate of adsorption is directly linked to the product of the initial dye concentration (C_o) and the dye concentration at any given time (C_t). The pseudo second-order kinetics equation is expressed as [29]:

$$t / C_t = 1 / (k_2 * qe^2) + t / q_e \quad (8)$$

Where k_2 represents the pseudo second order kinetics rate constant, and the amount of dye adsorbed at equilibrium is denoted by q_e. Plotting t/ C_t against time (t) reveals a linear relationship, with the slope of the line representing the rate constant, k_2.

The Weber-Morris model is another widely used model for adsorption kinetics. It is based on the assumption that the dye molecules diffuse through a solid boundary layer to access the solid surface adsorption sites. The Weber-Morris model equation is given as [30]:

$$(q_t / q_t) = 1 - e^{-kt} \quad (9)$$

Where the amount of dye adsorbed at time t is denoted by q_t, the amount of dye adsorbed at equilibrium is depicted by q_e, and k represents the rate constant of the Weber-Morris model. By plotting q_t / q_t against time (t), a curve can be observed, and the rate constant k can be determined.

These models provide insights into the adsorption kinetics of dyes onto solid surfaces and can be used to calculate various kinetic parameters for comparison and analysis. However, it is crucial to acknowledge that the choice of suitable model is reliant upon the particular adsorption system and the experimental parameters.

3. Result and discussion

3.1. Preparation mechanism

As in the present preparation, GL were taken, on the surface of which, MnO_2 was grown. Guava is a cheap and widely available fruit. Its leaves can act as a cellulose surface as has been reported in earlier studies [27]. This cellulose surface is rich in oxygenous groups (-OH, –COOH, –C═O), which attracts and binds the manganese ions present in the solution on its functional groups containing surface [27,29]. In this process, $KMnO_4$ acts as an oxidizing agent while $MnCl_2$ acts as a reducing agent and gives a redox reaction with each other in solution. Plant extracts may also have been released during this process, which helped increase the reaction rate by easily reducing $KMnO_4$ (Mn(VI)) to Mn(II) [31]. This process produces MnO_2 (which may be encapsulated with phytochemicals originated from plant extract of GL [31]) that precipitates on the leaf surface [28]. This overall process resulting in a strong interaction between the leave surface and the MnO_2 formed via electrostatic and non-electrostatic interaction, resulting in the formation of a composite. This preparation mechanism can be referred as Scheme 1. Further characterization studies have been conducted to prove this interaction.

3.2. Characterization

FT-IR Spectroscopy is an effective method to gain knowledge about the various functional groups present in the moiety. In this study, FT-IR investigation of GL extract and composite of MnO_2/GL was carried out which resulted in various characteristic absorption peaks in the functional group and fingerprint region from 4000 cm^{-1} to 400 cm^{-1} [32–36]. In the FT-IR spectroscopy analysis of GL (Fig. 1a; black line), A broad peak around 3200-3100 cm^{-1} appeared in the spectra indicating the presence of the hydroxyl group [29,30]. Another peak around 3000-2950 cm^{-1} is assigned for the -C-H stretching frequency of the alkyl group of carbon framework and a strong peak is observed around 1438 cm^{-1} which can be attributed to the O–H bending frequency of –COOH functional group (carboxylic acid) [36]. The MnO_2/GL FT-IR spectra (Fig. 1b; red line) showed all the absorption peaks identified in the GL carbon framework in addition to a broad peak that ranged from 516 cm^{-1} to 643 cm^{-1} that was indicative of metal-oxygen bonding [28,29].

The phase of MnO_2/GL can be confirmed from the XRD peaks at various 2θ values viz. 28.8°, 37.46°, 42.3°, 51.3°, and

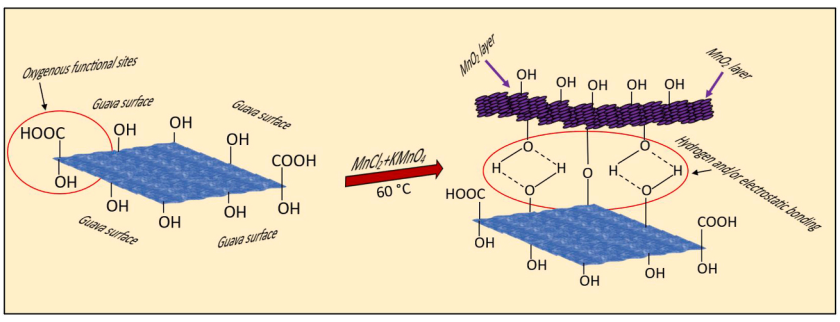

Scheme 1. Possible schematic illustration of the preparation of the MnO_2/GL.

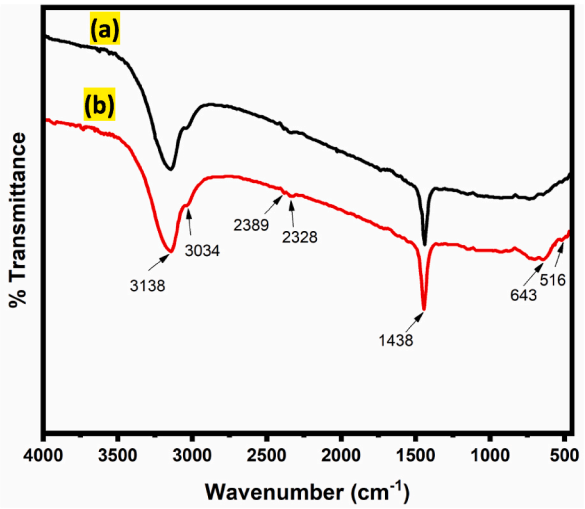

Fig. 1. FTIR analysis of (a) GL and (b) MnO_2/GL.

56.5° corresponding to the (002), (111), (301), (440), and (600) planes, respectively (Fig. 2a and b) [37,38]. The characteristic plane (111) was accounted for the δMnO_2 phase (JCPDS Card No. 42–1317) in the MnO_2/GL. XRD analysis shows the well agreement to the previous study for the confirmation of MnO_2/GL (Fig. 2) [29,37,38].

For further investigation, scanning electron microscopy (SEM) was employed for the imaging of the surface in order to investigate the morphology of the MnO_2/GL composite [39–41]. The SEM image (Fig. 3.) showcased the irregular growth of MnO_2 particles over the GL carbon framework. From the magnified SEM image, it can also be deduced that MnO_2 particles have formed aggregates. Thus, SEM confirms the porous structure of the composite having good contact of MnO_2 with GL.

The elemental composition of the prepared MnO_2/GL composite was analyzed via SEM-EDX spectroscopy. The EDX spectrum (Fig. 4.) shows the presence of C, O, and Mn in the composite. The occurrence of C and O is due to the GL carbon framework, whereas Mn originated from MnO_2 grown over the carbon framework of GL. Therefore, the SEM-EDX spectrum of MnO_2/GL established that MnO_2 particles had successfully grown in the carbon framework of GL.

Transmittance electron microscopy (TEM) (Fig. 5.) also verified the growth of particles by analyzing the surface on the nanometer scale. It demonstrated an uneven shape and distribution of MnO_2 particles having amorphous nature. It suggested that the agglomerated form of particles has an average size range from 3 to 5 nm. In addition, adsorption experiments were performed to ascertain the synthesized composite's effectiveness.

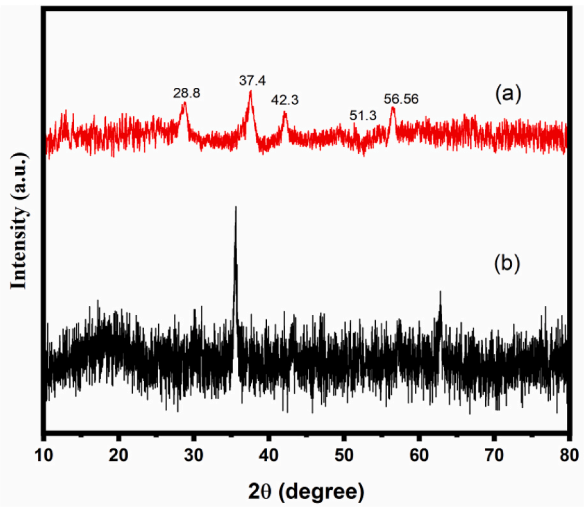

Fig. 2. XRD pattern of MnO_2/GL.

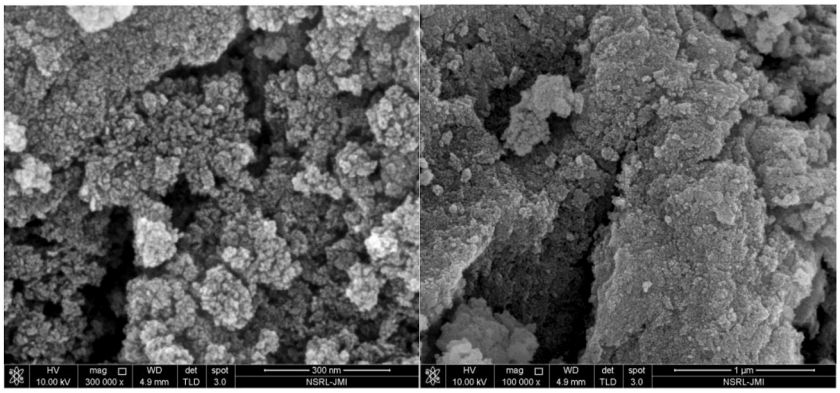

Fig. 3. SEM image of MnO_2/GL at different magnification.

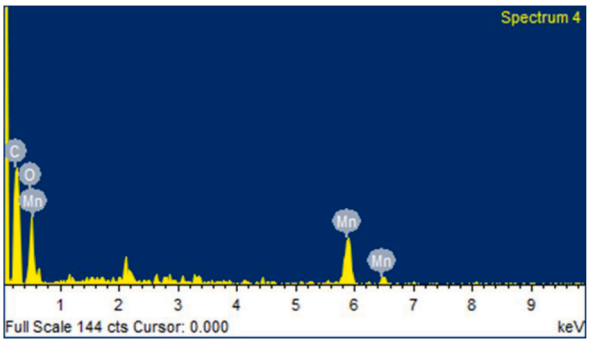

Fig. 4. Elemental analysis of MnO_2/GL using SEM-EDX graph.

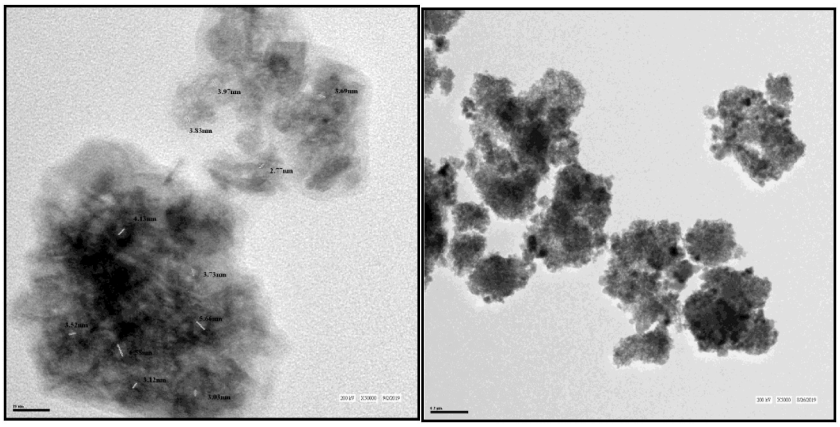

Fig. 5. TEM image of MnO_2/GL at different magnification.

3.3. Adsorption studies

The amount of NM, the pH of the solution, the concentration of dye, and the temperature all have a significant impact on the empty site interaction with dye molecules and, as a result, the adsorption effectiveness. Consequently, the effects of these parameters were investigated, and batch adsorption experiments were used to improve the efficiency [29,30].

3.3.1. Adsorbent dose optimization

The maximum adsorption of MB dye on MnO_2 decorated Guava leaves was found to be in presence of 1.5 g/L of the NM. As depicted in Fig. 6a, the maximum adsorption of ≈99.1 % of dye was observed at 1.5 g/L of adsorbent material. The increase in adsorption

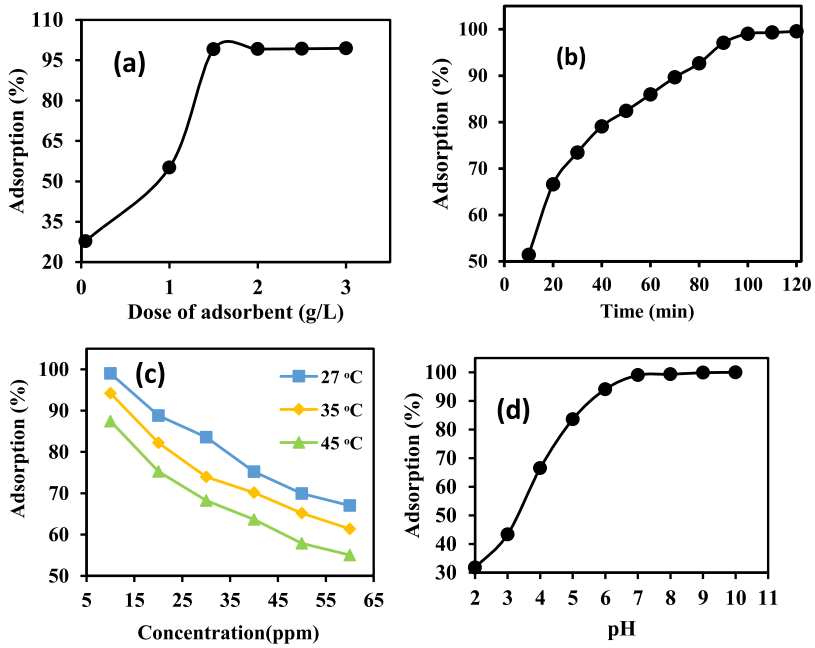

Fig. 6. Optimization of various parameters (a) adsorbent dose, (b) contact time, (c) dye concentration and solution temperature, (d) pH for the adsorption efficiency of MB.

efficiency with an increased dose of MnO_2/GL can be elicited based on the extent of available adsorption sites. With an increase in MnO_2/GL dose, the number of interactive sites increases, following which the removal efficiency also increases. The increase in adsorption is not significant enough with a further increase in the amount of adsorbent. Thus, an optimized dose of 1.5 g/L of the adsorbent was used in the further batch adsorption study.

3.3.2. Time optimization for adsorption process

The extent of MB dye removal is directly dependent on the time of exposure of adsorption sites to the dye. With greater residence time, more MB dye molecules interact with the vacant sites and consequently, the amount of dye removed increases. As evident in Fig. 6b. At an optimized time of 100 min, ≈99 % removal of dye was experienced. An appreciable increase in dye removal was not observed for further increase in time of residence. Thus, after a maximum occupancy (~99 %) of adsorption sites in 100 min, the adsorption process slowed down as an alternate pathway was required for further adsorption to take place. Therefore, the subsequent batch adsorption experiments were conducted at a time optimum of 100 min.

3.3.3. Optimization of concentration of MB dye solution

MB dye degradation was dependent on the concentration of MB present in the test solution as can be seen in Fig. 6c. The greater the concentration of MB in solution more is the NM required. Thus for 1.5 g/L of the adsorbent MnO_2/GL the maximum extent of adsorption was recorded for 10 ppm concentration of MB dye. With further increase in the amount of dye, the extent of adsorption decreased. This observation can be accounted for the lesser no. of available adsorption sites for greater no. of dye molecules.

3.3.4. Temperature effects on adsorption of MB dye

The temperature dependence of the dye removal process is evident in Fig. 6c. The adsorption experiments were conducted using a 10 ppm solution of MB dye in presence of MnO_2/GL at temperatures of 27 °*C*, 35 °*C*, and 45 °*C*. A perceptible decrease in adsorption was observed with an increase in temperature. This decreasing trend could be explained based on the interaction forces. There might exist some weak interactive forces between the adsorption sites and MB dye molecules. As the temperature rises, these interaction forces weaken and cause the dye molecules to desorb from the adsorbent's surface, resulting in a lower proportion of adsorption.

3.3.5. pH dependence of adsorption rate

The rate of adsorption and MB dye removal is dependent on pH as suggested in Fig. 6d. MnO_2/GL show a greater extent of adsorption at higher or basic pH. The extent of adsorption increased significantly from ≈31 % at a pH of 2 to nearly 99 % at a pH above 7. Studies suggested almost 100 % MB dye removal at a pH of 10. This could be clarified by comparing variations in ionization to changes in the solution's pH. With increase in pH, the hydroxide ion concentration increases which leads to the greater ionization of MB which is a cationic dye. A higher rate of adsorption results from an enhanced ionization rate, which increases the amount of MB dye removed [29,30].

3.3.6. Thermodynamics and isotherm studies

Thermodynamic studies of the MB dye degradation were conducted at three different temperatures. Using the thermodynamic parameters, the impact of temperature on the NC's adsorption capacity and, in turn, the effectiveness of dye degradation were investigated. The feasibility of MB dye degradation was analyzed by calculating the Gibbs free energy change involved in the adsorption process. Δ G^o value ranged from ~ −10 kJ mol^{-1} to −2 kJ mol^{-1} on increasing the temperature from 300 K to 318 K (Table 1).

The negative values of Δ G^o demonstrated that the adsorption process is viable. The low Gibbs free energy change (<−20 kJ mol^{-1}) was indicative of physical adsorption of dye on the NC surface. Also, the decrease in negative values of ΔG^o on increasing the temperature (300 K–318 K) represented the lower feasibility of reaction upon raising the temperature (Fig. 7). This can be accounted for based on a decrease in binding capacity of dye to the NC i.e., the attractive van der Waal's forces between the NC surface and the dye molecules might have weakened due to the higher thermal energy at elevated temperatures.

The enthalpy change, or ΔH value, was found to be negative (−139.25 kJ mol^{-1}), indicating that the adsorption process was exothermic [30]. Additionally, the entropy change was calculated to examine the reaction's spontaneity. It was evident from the calculation that entropy change was negative (−0.4304 kJ mol^{-1} K^{-1}). This negative value for ΔS can be attributed to the decrease in randomness due the dye fixation at the NC surface [29,30]. The values for ΔH and ΔS were calculated using the plot (Fig. 7) for variation of Δ G^o with temperature change.

Isotherm studies for a process form an important parameter to study the type of interaction adsorbate is undergoing with the adsorbent species. It helps in predicting the kind of layer formation (monolayer or multilayer), binding energy and to analyze whether the binding is homogenous or heterogenous. The previously mentioned objectives were realized for this adsorption process by studying three isotherm models (Langmuir, Freundlich and Temkin) (Fig. 8). Irwin Langmuir gave the Langmuir isotherm (L_m), which considers that neighboring molecules adsorbed on a surface do not influence the adsorption capacity of an adsorbate molecule. It supports the adsorption process to be chemisorption involving formation of monolayer only [30].

The Freundlich isotherm (F_r) suggests the multilayer heterogenous adsorption of adsorbate on the adsorbent surface [30]. Further, the Temkin isotherm model suggests a linear decrease in adsorption heat as the surface coverage increases. It also helps in calculation of the binding energy and the heat of adsorption [30].

Based on the obtained data of experimental and estimated Q_e values (Fig. 8) for these three models respectively at different temperatures, the best fitting model was found out. Average Range Error (ARE) was determined for each model at corresponding temperatures; lower the ARE more suited is the isotherm model. ARE was found to be minimum for Fr isotherm at both high and low temperature values (Table 2). This suggested that the best fitting isotherm model for the adsorption by MnO_2//GL NC is the Freundlich model. The n value ranges between ~1 and 4 which further affirms for the adsorption to be a multilayer adsorption. The k_F value was reported to range from 11.22 to 3.92 (mg g^{-1}) on raising the temperature which attests to the above-stated claim that the adsorption process is exothermic. k_F values predict the adsorption capacity, which in this regard decreases with an increase in temperature (Table 2).

Similar observation is reported in the L_m model as a decrease in **b** from 0.41 to 0.06 is found which confirms the declining adsorption affinity. Since from the L_m model, R_L values were found to range between 0 and 1, it could be inferred that MB adsorption on MnO_2/GL NC is feasible at all temperatures (in specified range). However, **ARE** was maximum for this model and thereby it is found to be least fitted model [30].

In the Tm model studies, A_T was found to be appreciably high (35.58) at lower temperature indicative of stronger bonding. The b_T values were found to be positive, but decreasing with an increase in temperature attesting to the inference that the process is exothermic in nature. It was observed that for higher temperatures **ARE** values were appreciably similar for Fr and Tm models. This suggested that the Temkin model is also suitable for the process at higher temperature. However, the Fr model was found to be best fitting at all temperatures.

Based on above-stated thermodynamic and isotherm studies it could be claimed that MB dye undergoes a multilayer physisorption on MnO_2/GL NC with a release of energy (exothermic) where the adsorption affinity decreases on elevating the temperature. The process involves a decrease in randomness due to incorporation of dye on the NC surface.

3.3.7. Kinetics and mechanism of MB adsorption

The kinetic and mechanistic studies were performed to study the rate of reaction and investigate the mechanism involved in the adsorption process. Adsorption processes are often observed to follow pseudo-first-order kinetics, and occasionally they follow pseudo-second order kinetics as well. Thus, using two distinct kinetic models—the pseudo-first order (PFO) and pseudo-second order (PSO) kinetic models—the kinetic pathway was verified.

Table 1
Results of thermodynamics of MB adsorption.

Temperature (K)	ΔG^o (kJ mol^{-1})	ΔH (kJ mol^{-1})	ΔS (kJ mol^{-1} K^{-1})
300	−10.46	−139.25	−0.4304
308	−6.11		
318	−2.64		

(Experimental conditions: pH = 7; Adsorption dose = 1.5 g/L; MB concentrations = 10–60 mg L^{-1}; Contact time = 120 min; Agitation speed = 200 rpm.).

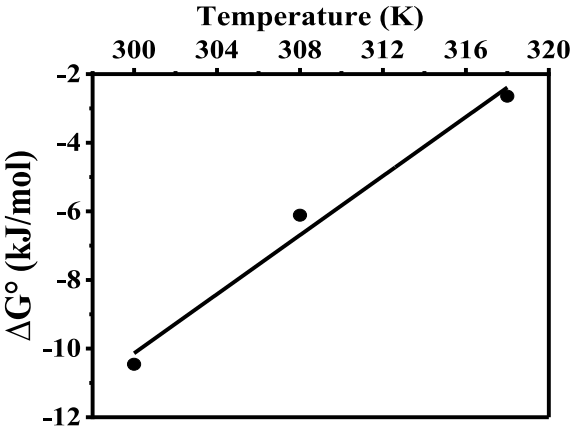

Fig. 7. Thermodynamic plot of methylene blue.

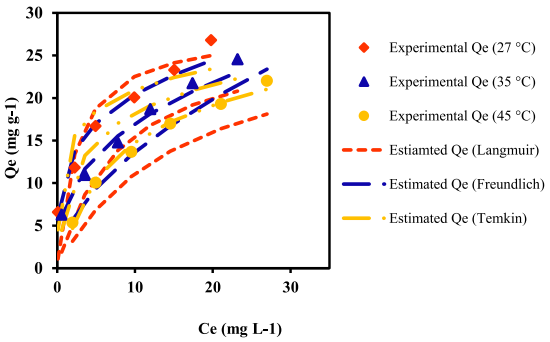

Fig. 8. Isotherm simulation plot of methylene blue adsorption. (For interpretation of the references to colour in this figure legend, the reader is referred to the Web version of this article.)

Table 2
Experimental observations for Isotherms studies for MB adsorption[a].

Order	Temp. (K)	Langmuir				Freundlich			Temkin		
		Q_o mg g^{-1}	b L mg^{-1}	R_L	ARE[b]	n	k_F mg g^{-1} (L mg^{-1})$^{1/n}$	ARE[b]	A_T	b_T	ARE[b]
1.	300	28.09	0.41	0.20	21.89	3.84	11.22	6.42	35.58	0.71	15.80
2.	308	27.93	0.13	0.44	22.42	2.76	7.38	4.86	4.36	0.54	13.37
3.	318	28.82	0.06	0.61	24.28	1.84	3.92	4.84	1.07	0.43	4.94

[a] Experimental conditions: pH = 7; Adsorption dose = 1.5 g/L; MB concentrations = 10–60 mg L^{-1}; Contact time = 120 min; Agitation speed = 200 rpm.
[b] ARE = Average range error.

The equations and significances related to these models are given in the theory section. Investigation of the most suitable kinetic model was attempted based on a linear plot for PFO and PSO (Fig. 9a and b). The plot for which the R^2 value is found to be the closest to unity is predicted to be the best-fitting kinetic model. The PFO and PSO rate constants k_1 and k_2 were comparable (Table 3). In addition, the standard error function χ should be less for a more appropriate model. Based on the linear plots it was established that the PSO model was the best-fitting model with regression factor $R^2 = 0.997$ which is close to unity. The standard error function χ was also found to be 0.115 indicating a greater agreement of experimental adsorption capacity (Q_e exp) with that of the expected theoretical values (Q_e cal). The χ value was comparatively less in PSO than that in the PFO model (0.334). Hence, the comparison of the PFO and PSO models suggested more suitability of the PSO model. This supported the presence of interactions between charged MB dye and functional groups of MnO_2/GL NC [29,30].

The rate-determining step as well as the mechanism pathway was investigated by plotting the Weber -Morris (WM) plot (Fig. 10). The rapid adsorption process suggested a possibility of intraparticle diffusion (IDP) but on the contrary, there are three different lines in the WM plot. This indicated the involvement of a three-step process in adsorption of MB dye on the NC surface. The green line passed

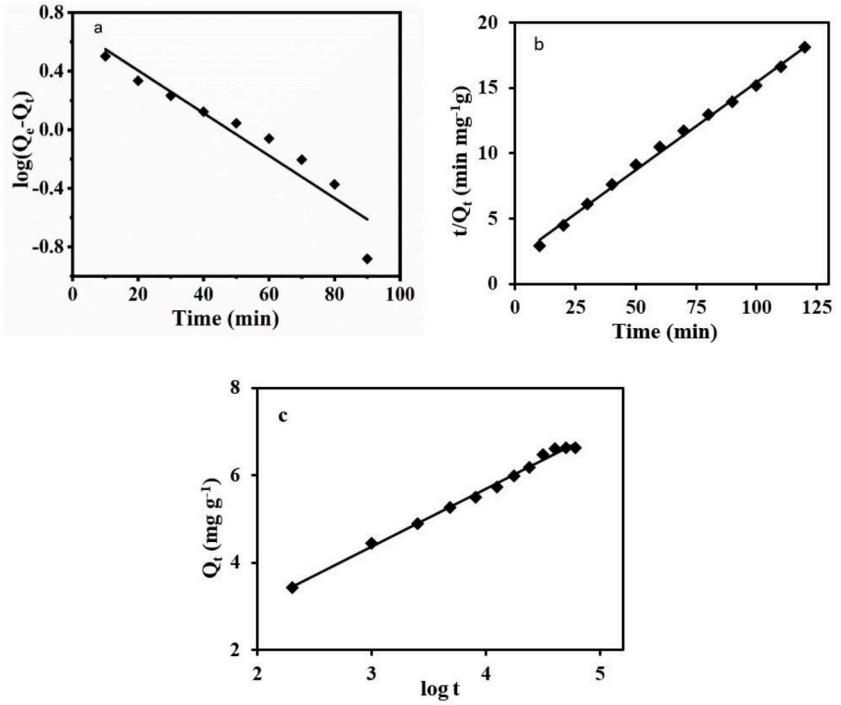

Fig. 9. Plots of (a) PFO kinetics and (b) PSO kinetics (Experimental conditions: pH = 7; Adsorption dose = 1.5 g/L; MB concentrations = 10–60 mg L^{-1}; Contact time = 120 min; Agitation speed = 200 rpm).

Table 3
Kinetics model studies for MB Adsorption.

Order	Pseudo First Order $Q_e$exp = 6.601					Pseudo Second Order $Q_e$exp = 6.601				
1.	k_1 0.033	$Q_e$cal 4.950	$\Delta Q_e^{\#}$ 1.651	R^2 0.912	χ 0.334	k_2 0.037	$Q_e$cal 7.457	ΔQ_e 0.856	R^2 0.997	χ 0.115

($\chi = (Q_e\text{exp} - Q_e\text{cal})/Q_e\text{cal}$, where $Q_e$exp and $Q_e$cal are the equilibrium experimental results and calculated value according to the model, respectively. #ΔQ_e is the difference between the Q_e estimated through the experiment ($Q_e$exp) and Q_e calculated by the kinetic model ($Q_e$cal).

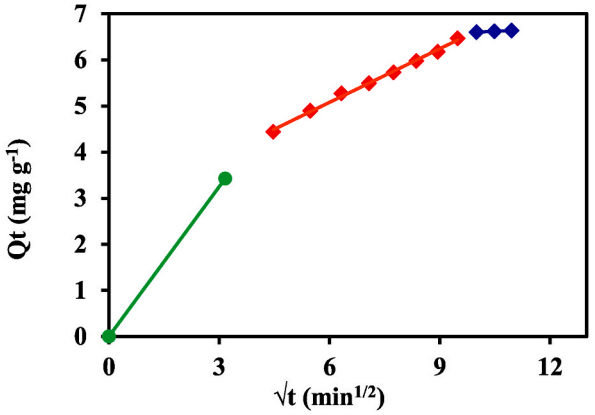

Fig. 10. WM for MB adsorption on to the NC (Experimental conditions: pH = 7; Adsorption dose = 1.5 g/L; MB concentrations = 10–60 mg L^{-1}; Contact time = 120 min; Agitation speed = 200 rpm).

through the origin with a high K_1 value indicating non-specific mass transfer in the time interval of 0–15 min. The red line represents thin-film diffusion in the second stage of the adsorption process in the time interval of 15–90 min. The blue line represents the IPD stage in the 90–120 min interval. Since the second and third stages had lower rate constant values, K_2 and K_3, as compared to the high K_1 value (Table 4) for the first mass transfer reaction, it was established that the second and third stages are the slower and hence rate-determining steps. Further, the boundary line thickness $C_2 < C_3$, which further suggested that intra-particle diffusion is the slowest step and hence the adsorption process is greatly dependent on the third IPD step. Both the K and C values were in agreement with the kinetic studies and suggested the reaction to be a PSO reaction proceeding via IPD as the rate-determining step [30].

This adsorption process occurred through electrostatic and non-electrostatic interactions between methylene blue and MnO_2/GL. As noted by FTIR, the present adsorbent has several functional groups such as hydroxyl, carboxylic, amide, and carbonyl that act as attractive sites. They interact with charged MB molecules. This interaction can be electrostatic or non-electrostatic as shown in Scheme 2 [42–45].

3.4. Reusability

The stability and reusability of the adsorbent is very important for any study, which makes the process economical. Therefore, the stability and reusability of the MnO_2/GL were also examined in this study. For this, the exhausted adsorbent (MnO_2/GL-MB) was regenerated by the desorption process and then the absorption–desorption process was repeated for several cycles. The acid and alkali solutions can be used to regenerate the MnO_2/GL-MB via desorption process. Since the present adsorption study showed that the present MnO_2/GL showed the lowest adsorption capacity at acidic pH for MB dye, it can be said that the dye loaded adsorbent MnO_2/GL-MB would show better desorption process at acidic pH. So, to regenerate the exhausted adsorbent, MnO_2/GL-MB (1.0 g) was stirred in 100 mL of 0.1 M HCl solution on a magnetic stirrer for 6 h. It was then centrifuged at 3000 rpm and washed with plenty of double distilled water. The regenerated MnO_2/GL was then dried and reused for further adsorption cycles under the same experimental conditions as before. The result of the reusability test is shown in Fig. 11. The regenerated MnO_2/GL showed better adsorption efficiency in the first two cycles, i.e., only 20 % of adsorption efficiency was lost by then, however, as the cycles increased, the removal efficiency decreased, and the efficiency was only up to 50 % after the fifth cycle. It can be said that the present adsorbent has proved to be a better adsorbent for the first two cycles. After the 5th cycle, XRD analysis of the regenerated MnO_2/GL was carried out to investigate the stability of the reused MnO_2/GL (Fig. S1). The XRD result showed that the existing MnO_2/GL remains stable even after the 5th cycle. The present adsorbent can be a better choice for water treatment process.

3.5. Leaching test

Leaching of NPs during wastewater treatment is a major problem which is toxic to water in the long-term exposure. The enrichment of NPs depends on the stability of the composite material (bonding between organic and inorganic contents). The process in which less leaching occurs depicts better adsorption process. To make the present study meaningful, leaching test was also done for this study. Such leaching experiment was performed from acidic pHs to the basic pHs. For the present leaching experiment, aqueous suspensions of MnO_2/GL (1.0 g of MnO2/GL in 100 mL of double distilled water) were kept for about 24 h after stirring for 6 h at various pH (2−10).

The sample solutions were centrifuged and the supernatant was analyzed by flame atomic adsorption spectroscopy (FAAS) to measure the dissolved manganese content in the solution. The result of this determination is shown in Fig. S2. The highest dissolved manganese content (~4.7–3.2 % at 2–6 pH) in the solution were found to be in acidic conditions. According to the results, leaching decreases as the pH increases. The dissolved manganese content in the neutral and basic pH remained quite low (2.8–2.6 %), indicating the stability of the present adsorbent. Therefore, MnO_2/GL has good stability at neutral pH [46].

4. Conclusion

A one-step co-precipitation approach was used to create the nano-bio-composite MnO_2/GL. Excellent adsorption activity of Methylene blue was demonstrated by the MnO_2/GL. According to the adsorption data, 1.0 g of MnO_2/GL was sufficient to remove 99 % of the Methylene blue content in 1 L of water containing 10 mg L^{-1}. Adsorption was most affected by water pH, being maximum in the pH range of 6–10. As the temperature rose, less adsorption occurred. A spontaneous and exothermic reaction was indicated by the measurements of ΔG^o, ΔS^o, and ΔH^o, which were all negative. The Freundlich isotherm and the adsorption data fit each other nicely. The process was governed by intra-particle diffusion and proceeded according to pseudo-second order kinetics. The adsorption mechanism was revealed through electrostatic and non-electrostatic interaction between methylene blue and MnO_2/GL. The

Table 4
Mechanism studies by Weber-Morris model.

S. No.	Webber-Morris Model								
	Green Line			Red Line			Blue Line		
	K_1	C_1	R^2	K_2	C_2	R^2	K_3	C_3	R^2
1.	1.083	0	1	0.388	2.747	0.996	0.037	6.234	0.998

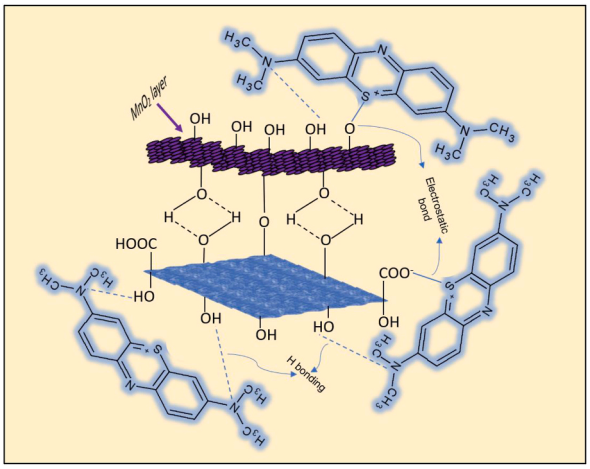

Scheme 2. Possible schematic illustration of mechanism of adsorption of MB onto MnO2/GL.

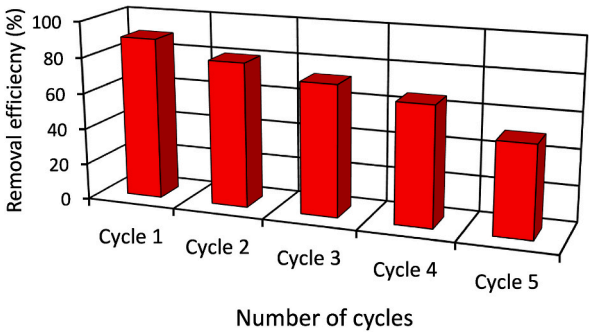

Fig. 11. Reusability test result for various cycles.

regeneration result suggested the efficient adsorption efficiency for two consecutive cycles. Leaching results revealed the stability of MnO_2/GL at neutral pH. Therefore, MnO_2/GL can be low-cost promising material for eliminating water pollution.

Data availability

The data that has been used is confidential.

CRediT authorship contribution statement

Noufal Komby Abdulla: Methodology, Investigation, Funding acquisition, Formal analysis, Data curation, Conceptualization. **Elham A. Alzahrani:** Writing – original draft, Methodology, Investigation, Formal analysis. **Poonam Dwivedi:** Data curation, Investigation, Methodology, Writing – review & editing. **Shruti Goel:** Writing – original draft, Methodology, Investigation, Formal analysis, Data curation. **Sumbul Hafeez:** Software, Methodology. **Mihir Khulbe:** Writing – review & editing. **Sharf Ilahi Siddiqui:** Writing – review & editing, Supervision, Conceptualization. **Seungdae Oh:** Writing – original draft, Supervision, Project administration, Funding acquisition.

Declaration of competing interest

The authors declare that they have no known competing financial interests or personal relationships that could have appeared to influence the work reported in this paper.

Acknowledgments

This work was in part supported (to S. O.) by Korea Environment Industry & Technology Institute (KEITI).

Appendix A. Supplementary data

Supplementary data to this article can be found online at https://doi.org/10.1016/j.heliyon.2024.e34267.

References

[1] D. Xu, S. Wu, A. Yan, Z. Chen, J. Xu, C. Gu, Y. Qi, S. Wu, Efficient recycling of sewage water in a polyester integrated industry: A case study, Desalin. Water Treat. 319 (2024) 100508.
[2] S. Bochynska, A. Duszewska, M. Maciejewska-Jeske, M. Wrona, A. Szeliga, M. Budzik, et al., The impact of water pollution on the health of older people, Maturitas 185 (2024) 107981.
[3] A. Ahamad, S.E. Siddiqui, P. Singh (Eds.), Contamination of water: health risk assessment and treatment strategies, Elsevier, 2021.
[4] I.B. Shehnaz, Prasher N. Ahmad, M. Ahmed, S. Raghuwanshi, V. Kumar, et al., Live biomass of rigidoporus vinctus: a sustainable method for decoloration and detoxification of dyes in water, Microorganisms 11 (2023) 1435.
[5] A. Góralczyk-Bińkowska, A. Długoński, P. Bernat, J. Długoński, A. Jasińska, Environmental and molecular approach to dye industry waste degradation by the ascomycete fungus Nectriella pironii, Sci. Rep. 11 (2021) 23829.
[6] S.I. Siddiqui, E.S. Allehyani, S.A. Al-Harbi, Z. Hasan, M.A. Abomuti, H.K. Rajor, et al., Investigation of Congo red toxicity towards different living organisms: a review, Processes 11 (2023) 807.
[7] G. Rathi, S.I. Siddiqui, S.A. Chaudhry, Chapter 10. Green material from plant source for the remediation of Methylene Blue dye: an emerging wastewater treatment technology, in: M. Yousuf (Ed.), Handbook of Textile Effluent Remediation, CRC press, 2018.
[8] G. Rathi, S.I. Siddiqui, Q. Pham, V.T. Nam, Nigella sativa seeds based antibacterial composites: A sustainable technology for water cleansing-A review, Sustain. Chem. Pharm. 18 (2020) 100332.
[9] E. Bistas, D.K. Sanghavi, in: StatPearls (Ed.), Methylene Blue, StatPearls Publishing, Treasure Island (FL), 2024 Jan [Updated 2023 Jun 26], https://www.ncbi.nlm.nih.gov/books/NBK557593/.
[10] Z. Wang, P. Yang, X. He, Q. Yu, Preparation of intercalated MXene by TPAOH and its adsorption characteristics towards U(VI), J. Radioanal. Nucl. Chem. 333 (2024) 1999–2014.
[11] L. Zhang, S. Jiang, Y. Jia, M. Zhang, J. Guo, Effects of Na+/H2O2 on nitrogen removal and sludge activity: Performance and mechanism, J Environ. Chem. Eng. 12 (2024) 113194.
[12] M.T. Yagub, T.K. Sen, S. Afroze, H.M. Ang, Dye and its removal from aqueous solution by adsorption: a review, Adv. Colloid Interface Sci. 209 (2014) 172–184.
[13] S. Wong, N.A. Ghafar, Ngadi, N.F.A. Razmi, I.M. Inuwa, R. Mat, N.A.S. Amin, Effective removal of anionic textile dyes using adsorbent synthesized from coffee waste, Sci. Rep. 10 (2020) 2928.
[14] N. Kumar, A. Pandey, Rosy, Y.C. Sharma, A review on sustainable mesoporous activated carbon as adsorbent for efficient removal of hazardous dyes from industrial wastewater, J. Water Proc. Eng. 54 (2023) 104054.
[15] A.M. Alsuhaibani, A.A. Alayyafi, L.A. Albedair, M.G. El-Desouky, A.A. El-Bindary, Synthesis and characterization of metal–organic frameworks based on thorium for the effective removal of 2,4-dichlorophenylacetic pesticide from water: batch adsorption and Box-Behnken Design optimization, and evaluation of reusability, J. Mol. Liq. 398 (2024) 124252.
[16] A. Almahri, K.S. Abou-Melha, H.A. Katouah, A.M. Al-bonayan, F.A. Saad, M.G. El-Desouky, A.A. El-Bindary, Adsorption and removal of the harmful pesticide 2,4-dichlorophenylacetic acid from an aqueous environment via coffee waste biochar: synthesis, characterization, adsorption study and optimization via Box-Behnken design, J. Mol. Struct. 1293 (2023) 136238.
[17] S.H. Alrefaee, M. Aljohani, K. Alkhamis, F. Shaaban, M.G. El-Desouky, A.A. El-Bindary, et al., Adsorption and effective removal of organophosphorus pesticides from aqueous solution via novel metal-organic framework: adsorption isotherms, kinetics, and optimization via Box-Behnken design, J. Mol. Liq. 384 (2023) 122206.
[18] H. Dabhane, S. Chatur, G. Jadhav, P. Tambade, V. Medhane, Phytogenic synthesis of gold nanoparticles and applications for removal of methylene blue dye: a review, Environ. Chem. Ecotoxicol. 3 (2021) 160–171.
[19] B. Fatima, B.A. Alwan, S.I. Siddiqui, R. Ahmad, M. Almesfer, M.K. Khanna, et al., Facile synthesis of cu-zn binary oxide coupled cadmium tungstate (Cu-znbo-cp-ct) with enhanced performance of dye adsorption, Water 13 (2021) 3287.
[20] B. Fatima, S. Siddiqui, R. Ahmed, S.A. Chaudhry, Preparation of functionalized CuO nanoparticles using Brassica rapa leave extract for water purification, Desalin. Water Treat. 164 (2019) 192–205.
[21] J. Aktar, M. Ray, Iron-polyphenol nanomaterial removes fluoride and methylene blue dye from water and promotes plant growth, J. Environ. Chem. Eng. 10 (2022) 107707.
[22] D.R. Vaddi, R. Malla, S. Geddapu, Magnetic activated carbon: a promising approach for the removal of methylene blue from wastewater, Desalination Water Treat. 317 (2024) 100146.
[23] G.J. Joshiba, P.S. Kumar, G. Rangasamy, P.T. Ngueagni, G. Pooja, G.B. Balji, et al., Iron doped activated carbon for effective removal of tartrazine and methylene blue dye from the aquatic systems: kinetics, isotherms, thermodynamics and desorption studies, Environ. Res. 215 (2022) 11431724.
[24] M.H. Kim, I.T. Jeong, S.B. Park, J.W. Kim, Analysis of environmental impact of activated carbon production from wood waste, Environ. Eng. Res. 24 (2 117) (2019) 117–126.
[25] M.S. Podder, C.B. Majumder, Bacteria immobilization on neem leaves/MnFe2O4 composite surface for removal of As(III) and As(V) from wastewater, Arab. J. Chem. 12 (2019) 3263–3288.
[26] S. Naseer, S. Hussain, N. Naeem, M. Pervaiz, M. Rahman, The phytochemistry and medicinal value of *Psidium guajava* (guava), Clin. Phytosci. 4 (2018) 32.
[27] N.K. Abdulla, S.I. Siddiqui, B. Fatima, R. Sultana, N. Tara, A.A. Hashmi, et al., Silver based hybrid nanocomposite: a novel antibacterial material for water cleansing, J. Clean. Prod. 284 (2021) 124746.
[28] N. Tara, S.I. Siddiqui, Q.V. Bach, S.A. Chaudhry, Reduce graphene oxide-manganese oxide-black cumin-based hybrid composite (rGO-MnO2/BC): a novel material for water remediation, Mater. Today Commun. 25 (2020) 101560.
[29] S.I. Siddiqui, O. Manzoor, M. Mohsin, S.A. Chaudhry, Nigella sativa seed based nanocomposite-MnO_2/BC: an antibacterial material for photocatalytic degradation, and adsorptive removal of Methylene blue from water, Environ. Res. 171 (2019) 328–340.
[30] S.I. Siddiqui, S.A. Chaudhry, Nanohybrid composite Fe_2O_3-ZrO_2/BC for inhibiting the growth of bacteria and adsorptive removal of arsenic and dyes from water, J. Clean. Prod. 223 (2019) 849–868.
[31] A.K.M.A. Ullah, M.M. Haque, M. Akter, A. Hossain, A.N. Tamanna, M.M. Hosen, et al., Green synthesis of Bryophyllum pinnatum aqueous leaf extract mediated bio-molecule capped dilute ferromagnetic α-MnO2 nanoparticles, Mater. Res. Express 7 (2020) 015088.
[32] S. Hafeez, L. Nebhani, Well defined and responsive amphiphilic block copolymers synthesized using TEMPO initiated thiol-ene reaction, Mater. Today Commun. 21 (2019) 100637.
[33] S. Hafeez, L. Barner, L. Nebhani, TEMPO driven mild and modular route to functionalized microparticles, Macromol. Rapid Commun. 39 (2018) 1800169.
[34] S. Hafeez, L. Nebhani, TEMPO driven thiol–ene reaction for the preparation of polymer functionalized silicon wafers, New J. Chem. 45 (2021) 9118–9129.
[35] S. Hafeez, V. Khatri, H.K. Kashyap, L. Nebhani, Computational and experimental approach to evaluate the effect of initiator concentration, solvents, and enes on the TEMPO driven thiol–ene reaction, New J. Chem. 44 (2020) 18625–18632.

[36] E.A. Alzahrani, P. Dwivedi, B. Fatima, S. Hafeez, S.I. Siddiqui, S. Oh, Cu-Zn coupled heterojunction photocatalyst for dye degradation: Performance evaluation based on the quantum yield and figure of merit, J. Saudi Chem. Soc. 28 (2024) 101858.
[37] Y. Zhai, X. Xu, H. Wang, X. Shi, D. Lei, Adsorption of copper on tri-aminofu nctionalized mesoporous delta manganese dioxide from aqueous solution, Water Sci. Technol. 71 (2015) 747–753.
[38] X. Wan, S. Yang, Z. Cai, Q. He, Y. Ye, Y. Xia, et al., Facile synthesis of MnO_2 nanoflowers/N-doped reduced graphene oxide composite and its application for simultaneous determination of dopamine and uric acid, Nanomaterials 9 (2019) 847.
[39] S. Hafeez, J. Jaishankar, P. Srivastava, L. Nebhani, Bactericidal materials prepared via conjugation of responsive polymers to cysteine, Mater. Today Commun. 26 (2021) 101813.
[40] S. Hafeez, Sulfur-based advance nanomaterials for water treatment, in: Contamination of Water, Academic Press, Elsevier, 2021, pp. 405–416.
[41] P. Yadav, S. Hafeez, J. Jaishankar, P. Srivastava, L. Nebhani, Antimicrobial and responsive zwitterionic polymer based on cysteine methacrylate synthesized via raft polymerization, Polym. Sci. 63 (2021) 505–514.
[42] M.G. El-Desouky, A.A. Alayyafi, G.A.A.M. Al-Hazmi, A.A. El-Bindary, Effect of metal organic framework alginate aerogel composite sponge on adsorption of tartrazine from aqueous solutions: adsorption models, thermodynamics and optimization via Box-Behnken design, J. Mol. Liq. 399 (2024) 124392.
[43] A.M. Alsuhaibani, A.A. Alayyafi, L.A. Albedair, M.G. El-Desouky, A.A. El-Bindary, Efficient fabrication of a composite sponge for Cr(VI) removal via citric acid cross-linking of metal-organic framework and chitosan: adsorption isotherm, kinetic studies, and optimization using Box-Behnken design, Mater. Today Sustain. 26 (2024) 100732.
[44] T.A. Altalhi, M.M. Ibrahim, G.A.M. Mersal, M.H.H. Mahmoud, T. Kumeria, M.G. El-Desouky, et al., Adsorption of doxorubicin hydrochloride onto thermally treated green adsorbent: equilibrium, kinetic and thermodynamic studies, J. Mol. Struct. 1263 (2022) 133160.
[45] A. Al-Hazmi, G. El-Zahhar, A.A. El-Desouky, M.G.M.A. El-Bindary, A.A. El-Bindary, Efficiency of Fe_3O_4@ZIF-8 for the removal of Doxorubicin from aqueous solutions: equilibrium, kinetics and thermodynamic studies, Environ. Technol. 45 (2022) 731–750.
[46] E. Matei, C. Predescu, A. Berbecaru, A. Predescu, R. Truşcă, Leaching tests for synthesized magnetite nanoparticles used as adsorbent for metal ions from liquid solutions, Dig. J. Nanomater. Biostruct. 6 (2011) 1701–1708.